doi:10.14311/ppt.2017.3.213
Plasma Physics and Technology **4**(3):213–224, 2017

MODELLING AND SIMULATION OF SF_6 HIGH-VOLTAGE CIRCUIT-BREAKERS - AN OVERVIEW ON BASICS AND APPLICATION OF CFD ARC SIMULATION TOOLS

F. Reichert[a,*], A. Petchanka[a], P. Freton[b], J.J. Gonzalez[b]

[a] *Siemens AG, Nonnendammallee 104, 13629 Berlin, Germany*
[b] *University Paul Sabatier, LAPLACE, 118 route de Narbonne, CNRS-UPS, 31062 Toulouse, France*
[*] frank.reichert@siemens.com

Abstract. The paper gives an overview on the basics of CFD arc simulation tools with respect to the simulation of the fluid mechanical processes in the interrupter unit of SF_6 high-voltage circuit-breakers at no-load and short-circuit switching-off processes. On the example of SF_6 self-blast circuit-breakers the complete process from the analysis of the switching-off process to the creation of a modular simulation model consisting of several sub models is illustrated. Details to the modelling in the particular sub modules and to the implementation are given. The capability of a CFD arc simulation tool based on the program package ANSYS/FLUENT is demonstrated on the basis of selected simulation results. Furthermore case examples for the application of the presented CFD arc simulation tool in the development process of high-voltage circuit-breakers are given.

Keywords: high-voltage circuit-breaker, CFD arc simulation tool, modelling, application.

1. Introduction

High-voltage circuit-breakers (HVCB) are exposed to several loads during operation. Figure 1 shows selected loads and the resulting stresses connected with high-voltage circuit-breakers [1]. The load by a continuous current leads due to the Ohmic heating of the current paths to a temperature rise and thus to a thermal stress. A short-circuit current leads to thermal stresses too and to mechanical stresses due to the high electromagnetic forces. Applying a voltage leads to a dielectric stress. Mechanical stresses can be also generated by loads at the terminals or seismic activities.

According to the requirements at its installation location high-voltage circuit-breakers have to handle different switching cases which lead to a mixture of dielectrical, mechanical and thermal stresses. In this context a CFD (Computational Fluid Dynamics) arc simulation tool should be able to simulate the gas flow processes inside the interrupter unit of high-voltage circuit-breakers during the switching-off process of short-circuit currents, see Figure 1. The CFD arc simulation tool should give information on the gas behaviour as the pressure build-up inside the interrupter unit and e.g. the distribution of gas temperature and density. Furthermore the CFD arc simulation tool should give information on the switching capacity for the different switching cases. Such information can be used in the development process of high-voltage circuit-breakers.

In this publication the basics of the modelling and simulation with respect to SF_6 self-blast circuit-breakers are given, which enable such a functionality of the CFD arc simulation tool. Based on the analysis

Loads		Stresses	Expected results from simulation
Continuous current		Thermal	
Short-time current		Thermal, Mechanical	
Voltage		Dielectrical	
Mechanics		Mechanical	
Switching	Switching-off of short-circuit currents (Terminal fault, Out-of-phase, Short-line fault)	Dielectrical, Mechanical, Thermal	Gas behaviour (pressure build-up, gas temperature and density), Switching capacity
	Switching of capacitive currents	Dielectrical	⇧
	Switching of small inductive currents	Dielectrical	CFD arc simulation tool

Figure 1. Loads, stresses and expected simulation results connected with high-voltage circuit-breakers.

of the switching-off process in Section 2.1 the overall physical system is identified which is based on the combination and interaction of several sub systems. In Section 2.2 the main aspects of the modelling in the separated sub systems are explained. Section 2.3 gives specific details to the implementation of CFD arc simulation tools. Considering the given information on modelling and implementation the set-up of a CFD arc simulation tool implemented in ANSYS/FLUENT is introduced in Section 2.4. In order to demonstrate the capability of this tool Section 2.5 presents selected simulation results. On the basis of three case examples it is shown in Section 3 how the introduced CFD arc simulation tool can be applied in the development process of high-voltage circuit-breakers.

Finally, the conclusions and an outlook are given in Section 4.

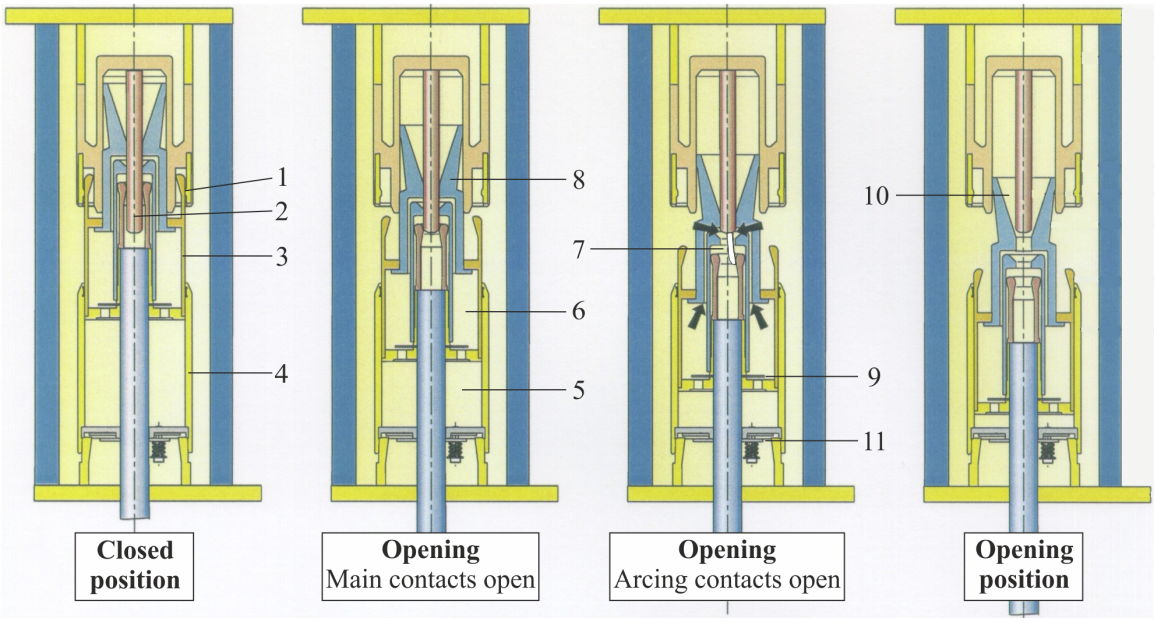

Figure 2. Illustration of variation of interrupter unit geometry during switching-off process.

2. Basics of modelling and simulation

2.1. Structuring of physical system of a SF_6 self-blast circuit-breaker

In case of SF_6 self-blast circuit-breakers the gas pressure needed for the flow of the arc extinguishing medium is created by the thermal energy of the arc itself. This is partially realized by a complex variation of the interrupter unit geometry during the switching-off process [2], see Figure 2. In the closed position the current flows over the main contacts (1). During the switching-off process the drive operates and the movable parts of the interrupter unit are moved downwards. By the opening of the main contacts the current commutates to the arcing contacts (2). Subsequently, the switching arc is ignited by the separation of the arcing contacts. Simultaneously, the cylinder (3) moves into the socket (4) which leads to the compression of the arc quenching gas inside of the compression volume (5). The gas flows through the heating volume (6) into the arcing volume (7) and quenches the arc. This behaviour of the gas flow is valid at the switching-off process of low-current arcs and during no-load operations. At the switching-off process of fault currents with significant current values the conditions change. In that case the strong Ohmic heating by the arc and the ablation of the insulating nozzle (made by polytetrafluoroethylene, PTFE) (8) lead to a high pressure build-up in the arcing volume forcing a hot gas flow into the heating volume. Thus the pressure increases inside the heating volume very strongly and valve 1 (9) closes supporting the pressure build-up furthermore. When the arcing contact enables the opening of the upper nozzle outlet (10) the gas from the heating volume flows back into the arcing volume and the switching arc is quenched in the current zero. To enable such a switching-off process a pressure equalization is realized by a second valve (11).

Following this analysis of the switching-off process the physical system of a SF_6 self-blast circuit-breaker can be identified, see Figure 3. As it can be seen from Figure 3 the physical system is based on the combination and interaction of the following sub systems

- Drive and switching mechanics
- Flow geometry
- Gas flow
- Switching arc
- Recovery after current zero

In the high-current phase the system input is represented by the current and the system output by the arc voltage. In the post arc phase the transient recovery voltage (TRV) acts as the system input and the recovery of the switching gap as the system output. The physical system can be coupled with an external sub system named External circuit, see Figure 3. In this case the output of the physical system is the ohmic resistance of the switching gap which is considered in the electrical network of the external circuit.

For each sub system the corresponding sub model can be developed. Details to the modelling are given in the following section.

2.2. Modelling for the various sub models

2.2.1. Drive and switching mechanics

The consideration of the operation of drive and switching mechanics depends on the features of the CFD program package in use. The illustrations in this paper concern the utilization of ANSYS/FLUENT. In this case the solver requires a velocity value in each time step to control the flow geometry variation. The

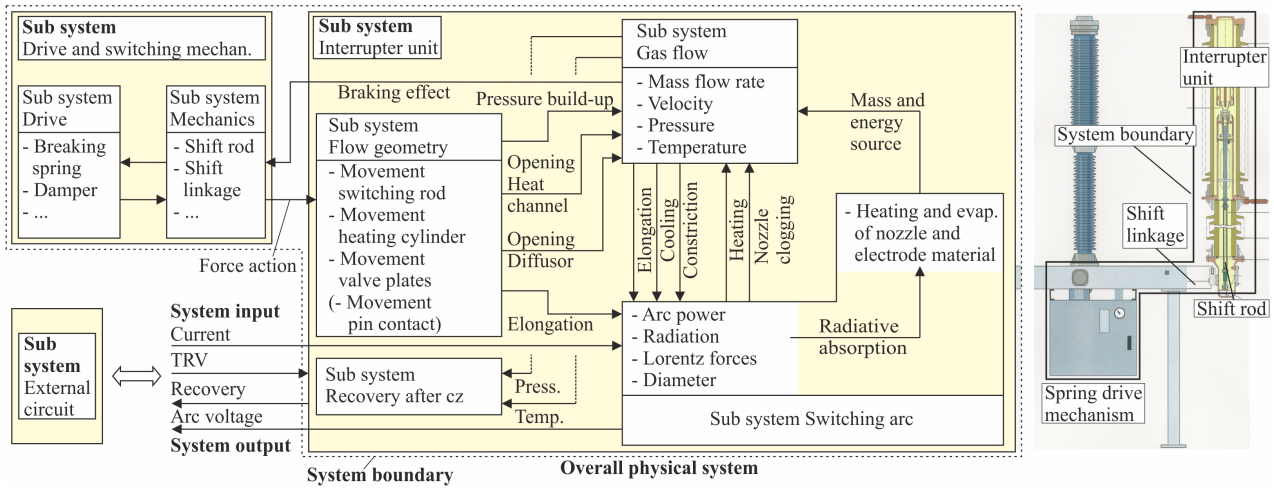

Figure 3. Physical system of a SF_6 self-blast circuit-breaker.

respective velocity value can be calculated by two different models

□ Interpolation model

□ Dynamic model

Interpolation model

In case of interpolation model a velocity course evaluated from measurements is provided to the CFD program at the beginning of the simulation. During the simulation an interpolation algorithm depending on simulation time delivers the velocity value in each time step. This is the most common approach in the literature. The important drawback of this approach is that the modelling does not take into account the feedback effect of the pressure build-up inside the interrupter unit on the operation of drive and switching mechanics.

Dynamic model

In case of dynamic model the pressure force determined from the flow simulation can be considered in the equation of motion which should reflect the operation of drive and switching mechanics. In [3], for example, the movement of movable parts is described using the following equation of motion

$$m\frac{\mathrm{d}^2x}{\mathrm{d}t^2} = F - k\cdot x - F_\mathrm{P} - f\left(x, \frac{\mathrm{d}x}{\mathrm{d}t}\right) \qquad (1)$$

In eq. (1), m is the weight of movable parts and driving part, x the displacement, F the driving force, k the spring constant, F_P the pressure force and f the damping force at displacement x and velocity $\mathrm{d}x/\mathrm{d}t$. With eq. (1) it is possible to investigate the influence of pressure build-up inside the interrupter unit on the stroke of movable parts.

The 1D approach according to eq. (1) cannot be used to describe the operation of drive and switching mechanics in a more complex system as depicted in Figure 4. The dynamic behaviour of such system can be described analytically using the Lagrangian mechanics. With the following assumptions

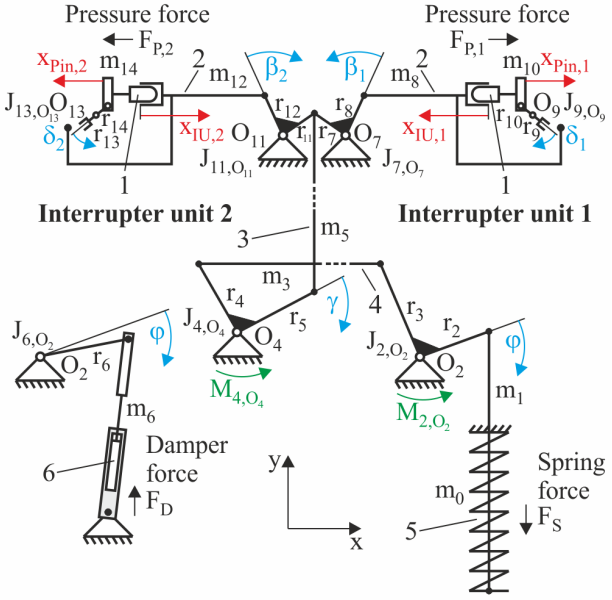

Figure 4. Scheme of switching mechanics for a circuit-breaker with two interrupter units (1: pin contact, 2: moving contact, 3: switching rod, 4: driving rod, 5: breaking spring, 6: hydraulic damper).

□ Pure translational movement of individual parts

□ No consideration of bouncing of individual parts

□ No consideration of changing in the kinematics of individual parts

the system can be modelled by a rigid body model. Despite the complexity of the system the degree of freedom is one and the mathematical model consists of only one differential equation for the angle φ. All other angles are linearly depending on φ. Due to the existence of conservative forces as well as non-conservative forces, the Lagrange equation is as follows

$$\frac{\mathrm{d}}{\mathrm{d}t}\left(\frac{\partial L}{\partial \dot{\varphi}}\right) - \left(\frac{\partial L}{\partial \varphi}\right) - Q = 0, \qquad (2)$$

whereas L is the Lagrange function according to

$$L = T - U. \tag{3}$$

In eq. (2), the term Q represents the generalised forces of non-conservative nature (e.g. the pressure force, the breaking torques and the force component from the hydraulic damper). In eq. (3), the term T summarises the parts concerning the kinetic energy as follows

$$T = m_0 \frac{(\dot{y})^2}{2} + \cdots = m_0 \frac{(r_2\dot{\varphi})^2}{2} + \cdots \tag{4}$$

and U concerning the potential energy (by the gravitational force on the switching rod and by the spring force) as follows

$$U = \frac{c_S}{2}(L_S - y)^2 + \cdots = \frac{c_S}{2}(L_S - r_2\varphi)^2 + \cdots . \tag{5}$$

The substitution of evaluated derivatives for the Lagrange function and the term for Q in eq. (2) leads to the equation of motion for the system:

$$\left(m_0 r_2^2 + \cdots\right)\ddot{\varphi} - c_S r_2 (L_S - r_2\varphi) + \cdots = 0. \tag{6}$$

The evaluation of eq. (6) in each time step delivers the angular velocity for the angle φ. Taking into account the mentioned linear relationships between φ and the other angles the interrupter unit velocity and the pin contact velocity are estimated in each time step. With these velocity values the variation of discretisation of the simulation model from time step to time step is updated in a continuous way. Note that via the term for the pressure force F_P (see Figure 4) the flow simulation and the simulation of the mechanical system are linked. Further details to the presented approach can be found in [4, 5].

2.2.2. Flow geometry

As mentioned in Section 2.1 the interrupter unit geometry changes notably during the switching-off process. The CFD arc simulation tool should be able to handle such a complex variation of the flow geometry, including the mesh modification, during flow simulation. In this context the elimination or generation of cells near to moving boundaries (Layering mesh method), the sliding of adjacent parts of the mesh relative to each other (Sliding mesh method) and the remeshing in separated regions (Remeshing mesh method) should be at least possible. Figure 5 illustrates a typical variation of solution domain and mesh between closed and opening position which was realized using these features with ANSYS/FLUENT. The illustration in Figure 5 shows e.g. the separation of pin and tube contact, the decreasing of the compression volume and the movement of the valve plate (valve 1) between heating and compression volume.

The movement of the valve plate should be controlled depending on the acting pressure force and in case of the pressure release valve additionally depending on a spring force on the plate. The respective

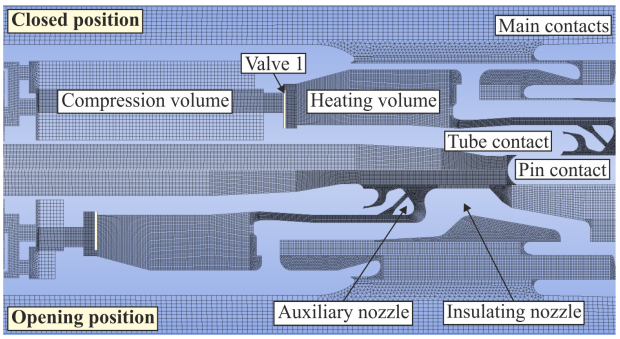

Figure 5. Illustration of mesh modification during switching-off process.

plate velocity v_{pl} can be calculated by the following equation of motion

$$v_{\mathrm{pl}}^{t+\Delta t} = v_{\mathrm{pl}}^{t} + \frac{\Delta t}{m_{\mathrm{pl}}} F_{\mathrm{pl}} \tag{7}$$

whereas m_{pl} is the plate mass. The term F_{pl} represents the acting pressure force and as mentioned in case of the pressure release valve the sum of acting pressure force and spring force.

2.2.3. Gas flow

The gas flow in the interrupter unit of high-voltage circuit-breakers has some unique characteristics. Independent from the circuit-breaker type, puffer or self-blast breaker, a changing pressure drop between inlet and outlet of the nozzle configuration is generated by piston-like geometries and by the switching arc during the switching-off process. The implications of this for the gas flow are as follows

- ☐ Starting flow process with low velocities (Mach number $M < 1$)
- ☐ Generation of compression shocks with changing localization
- ☐ Propagation of expansion and shock waves
- ☐ Flow degeneration at the end of switching-off process

The CFD arc simulation tool must be capable to reflect such a flow behavior. The respective functionality can be verified, for example, by the simulation of the stationary flow in a Laval nozzle and by the simulation of the transient flow in a shock tube. In [5] this verification process is illustrated for the CFD program package ANSYS/FLUENT.

2.2.4. Switching arc

In [6] the most important physical phenomena that have to be considered in the simulation of gas circuit-breakers are summarized. Based on this summarization the relevant phenomena for the modelling and simulation of ablation controlled arcs in the interrupter unit of high-voltage circuit-breakers can be identified as follows:

- ☐ Compressible flow including friction and turbulence

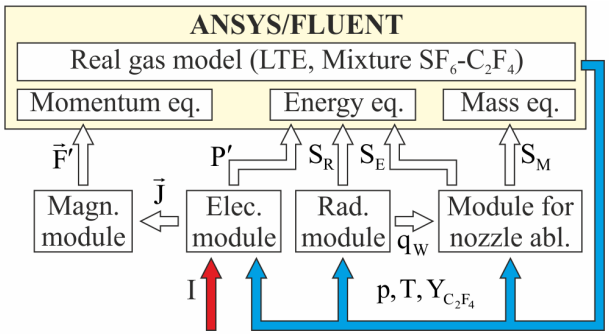

Figure 6. Link of conservation equations and sub models via source terms, vectorial and scalar quantities.

☐ Radiation transfer

☐ Ablation of nozzle wall material (C_2F_4)

☐ Electrode evaporation (WCu)

☐ Multi species transport (SF_6, C_2F_4, W, Cu)

☐ Electromagnetism

In the literature a distinction is made between an integral and a differential approach for the modelling of ablation controlled arcs [7].

In the intergal approach the switching arc is assumed as cylindrical plasma column with uniform temperature surrounded by an isothermal and non-conducting layer of ablated nozzle-vapour. This so-called two-zone model requires the input of several integral parameters derived from experimental data, see e.g. [8] or [9], or from CFD simulations, see e.g. [10]. The model delivers as the main predictions the arc axis temperature, the central pressure, the arc voltage, the arc radius and the ablating mass flux and can be used to describe the mass and energy sources in a CFD arc simulation, see e.g. [11].

In the more general differential approach the switching arc is described by a set of differential equations. In doing so the switching arc is integrated in the flow simulation using several source terms in the conservation equations which are evaluated by the solution of the respective differential equations. As an example Figure 6 shows a possibility for the implementation of an ablation controlled arc taking into account the ablation of nozzle wall material.

The module for nozzle ablation reproduces the heating and vaporization of nozzle material and delivers both a source term S_M in the mass equation and a source term S_E in the energy equation depending essentially on the ratio of wall radiative flux and effective specific ablation enthalpy of PTFE. A detailed description of the modelling in this module can be found in [12]. The module was further improved in [13] to take into account the nozzle wall deformation due to ablation.

The radiative transfer inside the switching arc and into its environment is reflected by the source term S_R in the energy equation. This source term is calculated in the radiation module. The most commonly used radiation models are the semi-empirical model based on the net emission coefficient (NEC) [14], the two standard methods for solving the radiative transfer equation (RTE), the model based on the spherical harmonics method (P1 model) [15] and the model based on the discrete ordinate methode (DO model) [16] or a combination of P1 and DO model [17]. Furthermore the radiation module provides the wall radiative flux q_W which is necessary for the calculation of nozzle ablation.

The source term P' in the energy equation for the consideration of the Joule effect is calculated in the electric module. In the most cases this source term is evaluated solving the potential scalar equation with appropriate boundary conditions, see e.g. [6] or [18].

The self-induced magnetic field due to the current flow is calculated in the magnetic module using the current density vector $\vec{J}$ provided from the electric module. Several approaches exist to calculate the self-induced magnetic field such as the Maxwell-Ampere formulation [19], the Biot & Savart formulation (BF) [20], the vector potential approach (VP) [21] or a combination of BF and VP [18]. From the self-induced magnetic field the Lorentz force vector $\vec{F'}$ can be deduced whose components represent the respective source terms in the momentum equations.

To solve the plasma flow the thermodynamic and transport properties of the arc plasma must be provided to the flow solver of ANSYS/FLUENT. This is realized by a real gas model for the mixture SF_6 - C_2F_4 based on the assumption of local thermodynamic equilibrium (LTE). The scalar quantities pressure p, temperature T and mass fraction $Y_{C_2F_4}$ calculated by ANSYS/FLUENT represent the input variables to the module for nozzle ablation, the radiation module and the electric module. A further input variable to the electric module is the current I.

The plasma flow is strongly governed by turbulence effects. The Prandtl mixing length model and the realizable $k-\varepsilon$ model are the most frequently used turbulence models in HVCB geometries. The Prandtl mixing length model is validated for the description of turbulence in the arc core region, see e.g. [22]. In [23], it is shown that the realizable $k-\varepsilon$ model clearly describes the flow conditions inside the heating volume compared with experimental results. The two models were compared in [24] and it was concluded that the realizable $k-\varepsilon$ model represents a reliable option to describe the turbulent flow inside the entire HVCB geometry.

2.2.5. Recovery after current zero

Concerning the modelling for this sub model it is necessary to distinguish between the behaviour at terminal fault (TF) and the behaviour at short-line fault (SLF).

Behavior at terminal fault

At a TF interruption the switching gap fails by

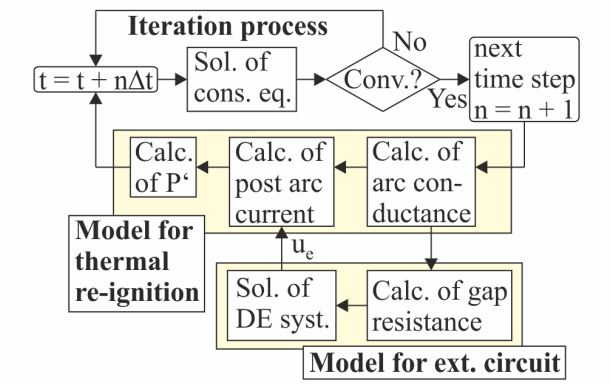

Figure 7. Flow chart for the simulation in the post arc phase at SLF interruption.

dielectric breakdown. Owing to its simplicity, the most commonly used approach for the study of the dielectric breakdown probability is the utilization of the so-called dielectric criterion k according to eq. (8) (see e.g. [25])

$$k = \frac{E_{\text{geom}}}{E_{\text{cr}}}. \tag{8}$$

Values for k greater than 1 characterize a high dielectric breakdown probability. For the estimation of k, an electrostatic field simulation is carried out at the same time as the flow simulation. The geometric electric field E_{geom} is evaluated from the simulated distribution of the electrostatic potential depending on the TRV which is applied between pin and tube contact after current zero. Using the results from the hot gas flow simulation after current zero, the critical electric field E_{cr} is calculated. For this purpose a pre-calculated data bank for the critical electric field depending on pressure, temperature and mass fraction must be provided to the flow simulation [26]. A more complex approach can be found in [27]. Here, a prediction method is presented which is built on spatial integration of critical and geometric electric field along several integration paths starting from the pin tip.

Behavior at short-line fault

At a SLF interruption the switching gap fails by thermal re-ignition due to the very fast rise of the TRV. Several approaches for the evaluation of the SLF interruption capability exist in the literature. For instance in [28] the trend of the post arc current calculated with different constant rises of recovery voltage is taken to evaluate the SLF interruption capability. In [29] a SLF interruption performance index is used which combines the pressure in the heating volume and the density above the arc zone.

Another possibility for the evaluation of the SLF interruption capability is given by an approach based on the coupling of a model for the thermal re-ignition and a model describing the transient response of an external circuit (e.g. high-voltage circuit) [30]. According to Figure 7 the solution of the equation system

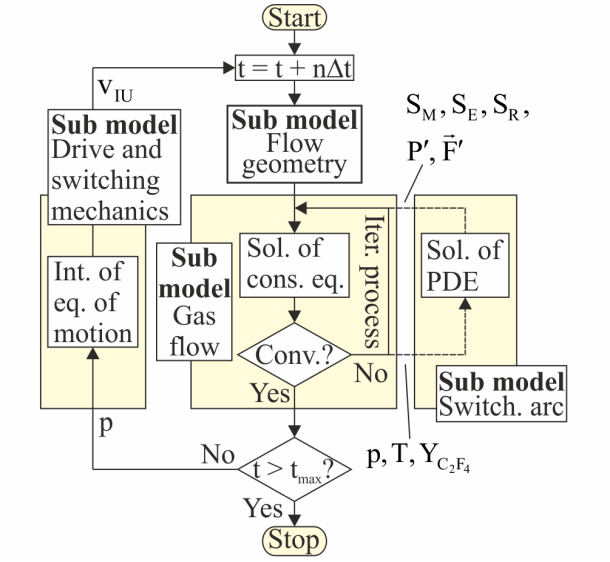

Figure 8. Flow chart for the simulation in the high current phase.

for the circuit in the model for the external circuit delivers the TRV u_{e} which is used in the model for the thermal re-ignition to calculate the post arc current and finally the source term in the energy equation P'. The simulated trend of the TRV can be used to evaluate the SLF interruption capability. Thus it is possible to visualize the simulated switching capacity of the regarded circuit-breaker in diagrams similar to test protocols.

2.3. Implementation of CFD arc simulation tools

Essentially, there are two main possibilities for the implementation of CFD arc simulation tools

- ☐ Framework with one CFD solver (Finite volume (FV) formulation)
- ☐ Framework with different solvers (FV formulation and finite element (FE) formulation)

Framework with one CFD solver

Figure 8 illustrates this framework. As it can be seen from Figure 8 the sub model Drive and switching mechanics is called at the end of the iteration process at each time step. Taking into account the simulated pressure distribution p the equation of motion is intergrated. This integration delivers the velocity of the movable parts of the interrupter unit v_{IU} which is used in the sub model Flow geometry to update the solution domain discretisation at the beginning of the new time step. After the discretisation manipulation the iteration process for the solution of the conservation equations and the partial differential equations describing the switching arc is started. As the data exchange between the sub model Gas flow and the sub model Switching arc is carried out at each iteration step a strong coupling between both sub models is achieved.

Framework with different solvers

As examples for this framework the simulation system using the coupling server MpCCI and the program package STAR-CCM+ should be named here.

In the first approach the data exchange and interpolation between the two customized commercial codes ANSYS/EMAG (FE solver) and ANSYS/FLUENT (FV solver) is realized by the coupling server MpCCI [31]. The ANSYS/EMAG solver is used to solve the electric and magnetic equations. The conservation equations as well as the radiation equations are solved by means of the ANSYS/FLUENT solver. Additonal sub models for e.g. electrode erosion and wall ablation are implemented using the programming interface of ANSYS/FLUENT.

According to [32] STAR-CCM+ innately provides a data mapper functionality for coupling of FE and FV solver. The gas flow and the electrical current are simulated on a polyhedral grid using the FV solver. The magnetic field is simulated on a standard shape finite element grid by means of the FE solver. To couple both solvers e.g. the source current density $\vec{J}$ is mapped onto the FE grid and the magnetic flux density $\vec{B}$ onto the FV grid.

2.4. Set-up of a CFD arc simulation tool based on ANSYS/FLUENT

The simulation results presented in this contribution have been achieved with the following set-up for the CFD arc simulation tool:

- ☐ ANSYS/FLUENT version 15
- ☐ Valve model
- ☐ Drive model
- ☐ 2 Species SF_6 - C_2F_4 real gas mixture model
- ☐ Realizable $k-\varepsilon$ model
- ☐ Non-grey DO model (7 bands)
- ☐ Switching arc model
- ☐ SLF or TF interruption model
- ☐ No consideration of electrode evaporation

2.5. Selected simulation results

In order to demonstrate the functionality of the presented CFD arc simulation tool selected simulation results are visualized in the following sub sections.

2.5.1. Simulation of the switching-off process in a model chamber

For the purpose of tool validation a model chamber has been assembled. The arc quenching area of the model chamber is presented in Figure 9. The slit in the insulating nozzle enables the access for optical emission spectroscopy (OES) measurements from which radial temperature distributions have been evaluated [33]. Besides the spectroscopic measurements, the stroke of moving contact, the arc voltage and the pressure build-up in the arc and heating volume have been measured.

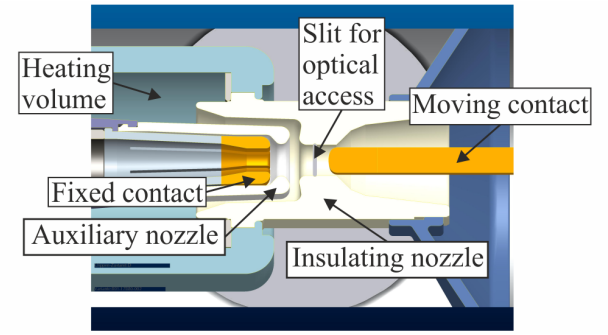

Figure 9. Arc quenching area of model chamber.

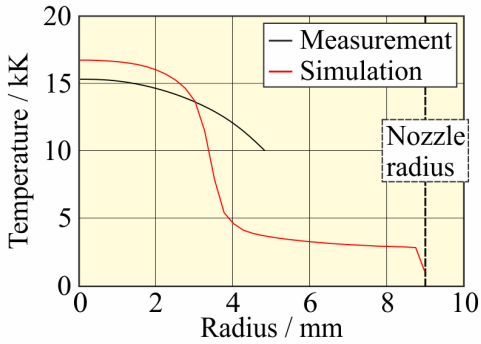

Figure 10. Comparison of radial temperature profiles.

By means of the CFD arc simulation tool the switching-off process in the model chamber has been simulated for an interrupting current with a root mean square (rms) value of $I_{\mathrm{rms}} = 10\,\mathrm{kA}$ and an arcing time of $t_{\mathrm{arc}} = 10\,\mathrm{ms}$. Details on the set-up of the CFD arc simulation tool can be found in [34].

In Figure 10 the simulated temperature profile is compared with the temperature profile evaluated from the OES measurements. The temperature profiles are compared at the time instant corresponding to an electrical current of $I_{\mathrm{instant}} = 1.7\,\mathrm{kA}$. As it can be seen from Figure 10 there is a good agreement between the simulated and the measured temperature profile validating the CFD arc simulation tool. The presented simulated temperature profile characterizes that there is no wall stabilization of the arc at the regarded time instant. Indeed, the temperature profile width is about 3 mm in contrast to the insulating nozzle radius of 9 mm. Assuming the square root dependence of arc core radius from electrical current, the arc wall stabilization should occur at currents higher than 15 kA.

2.5.2. Influence of nozzle degradation on pressure build-up

It is well known that insulating and auxiliary nozzle degrade during successive interruptions influencing arc power and pressure build-up inside the interrupter unit. To show the capability of the presented CFD arc simulation tool with respect to the reflection of

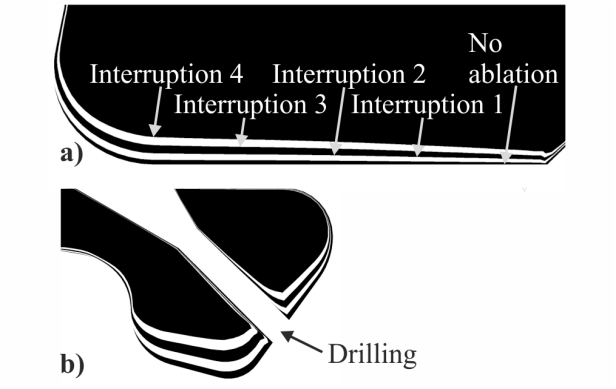

Figure 11. Degradation of the throat of the insulating nozzle (a) and of the nose part of the auxiliary nozzle (b).

this aspect a test series consisting of a set of four interruptions at $I_{\mathrm{rms}} = 25, 30, 35$ and 40 kA have been simulated [13]. After the simulation of the respective on-load switching-off process a no-load switching-on process has been simulated to reach the closed position of main and arcing contacts. As a result of this simulation sequence Figure 11 shows the accumulative wall degradation of insulating and auxiliary nozzle. The remarkable change in the shape of the nozzles can be clearly seen. The throat of the insulating nozzle takes on a conical profile instead of a cylindrical one and its cross-section increases. The part of the auxiliary nozzle near the moving contact becomes smaller. The drilling in the auxiliary nozzle changes its shape and becomes larger too. These changes in the geometry of the PTFE nozzles can also be observed in experiments.

The consideration of the accumulated PTFE nozzle deformation is essential for the simulation of the gas flow inside the interrupter unit. The difference between the pressure build-up trends simulated under the assumption of original and degraded nozzle geometries becomes much more remarkable with the increase in the number of interruptions in the test series and with the increase in the current. For the 4th interruption at the current $I_{\mathrm{rms}} = 40$ kA the comparison of the pressure build-up in the heating volume is presented in Figure 12. The pressure build-up obtained with the degraded nozzle geometry is in very good agreement with the measurements. The simulation with the original nozzle geometry overestimates the pressure build-up very strongly. This behaviour can be explained as follows:

- The flow cross-section inside the PTFE nozzles increases remarkably due to the accumulated PTFE nozzle degradation, as demonstrated in Figure 11. This leads to a faster escape of hot gas from the arcing volume decreasing the pressure here. The smaller amount of hot gas flowing to the heating volume results in a smaller pressure build-up. In the case of the simulation with original nozzle geoemtry this phenomenon takes no place resulting in a too high pressure build-up.
- The inner diameter of the insulating nozzle increases due to ablation. The amount of the ablated PTFE is smaller in the case of degraded nozzle geometry in comparison with the case of original nozzle geometry. This leads to the increase in the diameter of the plasma column. Thus the arc power is reduced resulting in a decreased pressure build-up.

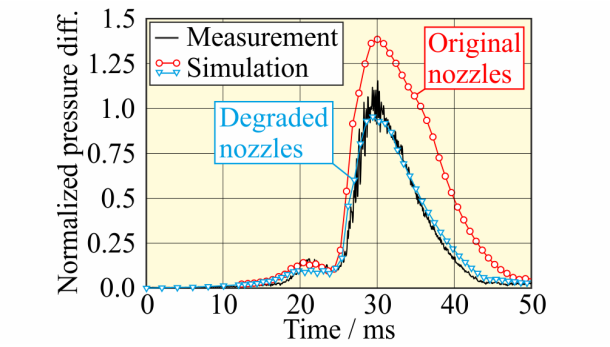

Figure 12. Pressure build-up in the heating volume depending on nozzle contours.

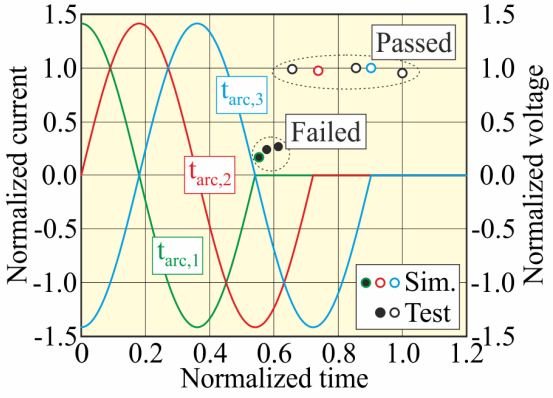

Figure 13. Current trends and peak values of TRV.

2.5.3. Evaluation of switching capacity at SLF interruption

With the approach presented in Section 2.2.5 the SLF interruption capacity of a real SF_6 self-blast circuit-breaker has been investigated for a complete test series consisting of the switching-off process at short arcing time ($t_{\mathrm{arc},1}$), medium arcing time ($t_{\mathrm{arc},2}$) and long arcing time ($t_{\mathrm{arc},3}$) [30]. Figure 13 shows the respective current trends which were multiplied for the simulation by a current rms value of $I_{\mathrm{rms}} = 36$ kA. The time line of Figure 13 is normalized by the maximum arcing time and the voltage values by the maximum peak value of the TRV in the test series. Additionally the measured and simulated peak values of the TRV are depicted in comparison. As it can be seen the simulation model predicts the switching capacity very similar to the test series.

From Figure 13 it can clearly be seen that the conditions with respect to a successful switching-off process are clearly worse at $t_{\mathrm{arc},1}$ than at $t_{\mathrm{arc},2}$. The

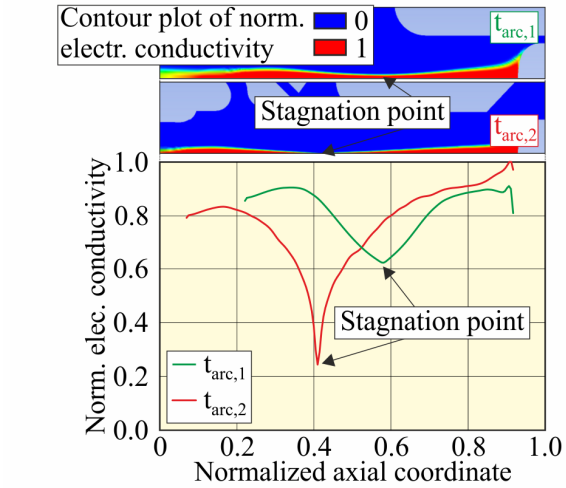

Figure 14. Axial distribution of electrical conductivity at current zero.

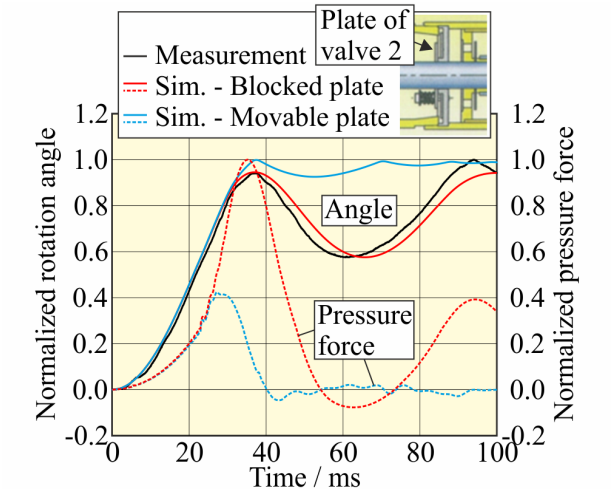

Figure 15. Course of rotation angle and pressure force.

pressure build-up in the heating volume during the high-current phase is clearly lower at $t_{arc,1}$ which leads to a reduced gas flow from the heating volume to the arcing volume at current zero. Thus there are lower values of pressure and higher values of temperature in the arcing volume at $t_{arc,1}$ at current zero leading (especially in the stagnation point) to higher values of the electrical conductivity in the arcing volume and to a greater diameter of the remaining arc channel, see Figure 14. The higher values of the electrical conductivity and the greater diameter of the remaining arc channel in case of $t_{arc,1}$ lead to a lower resistance of the contact gap in and just after the current zero when the contact gap is stressed by the TRV. By this reason the TRV causes a post arc current through the remaining arc channel high enough to heat up the leftover plasma and finally the thermal re-ignition of the contact gap.

3. Application of CFD arc simulation tools

CFD arc simulation tools are able to support the development process of high-voltage circuit-breakers. In this connection their application can yield benefits for the following selected aspects:

- ☐ Generation of a better understanding of physical processes in the interrupter unit during the switching-off process
- ☐ Improvement of existing interrupter unit designs
- ☐ Development of new interrupter unit designs
- ☐ Savings in costs for assembling and performance testing of prototypes
- ☐ Savings in development time

To illustrate some of these aspects three case examples are highlighted in the following sections.

3.1. Detection of a mechanical failure in the interrupter unit

By the utilization of the CFD arc simulation tool it is possible to locate mechanical failures in the interrupter unit. Figure 15 shows an experimental rotation angle (black curve, measured during SLF interruption at O_4 in Figure 4) which characterizes an unintended backward movement of the moving contact during the switching-off process. The cause for the depicted strong backward movement of the moving contact could be detected by several CFD arc simulations in form of a blocked plate of valve 2 (see top right in Figure 15). By the blocked valve plate a very strong pressure increase in the compression volume is generated resulting in an excessive pressure force which decelerates the drive and causes the strong backward movement (see red curves in Figure 15). In the CFD arc simulation with a moveable plate of valve 2 the pressure force reaches only about 40% resulting in a very slight backward movement (see blue curves in Figure 15). Using these results the design near valve 2 was improved and the problem of the strong backward movement of the moving contact did no longer exist in ensuing tests.

3.2. Reduction of the transient pressure rise at a rupture disc

Selected circuit-breaker types feature rupture discs for pressure equalization in case of fault arcs. In this connection the rupture disc must not operate during a regular switching-off process. That means that the transient pressure rise at the rupture disc caused by a switching-off process of short-circuit currents must not exceed the opening pressure of the rupture disc. The CFD arc simulation tool can be used in the process of rupture disc qualification. In a first simulation at an asymmetrical TF interruption the transient pressure rise at the rupture disc has been simulated for a first design (design 1). From the black curve in Figure 16 it can be seen that the maximum value

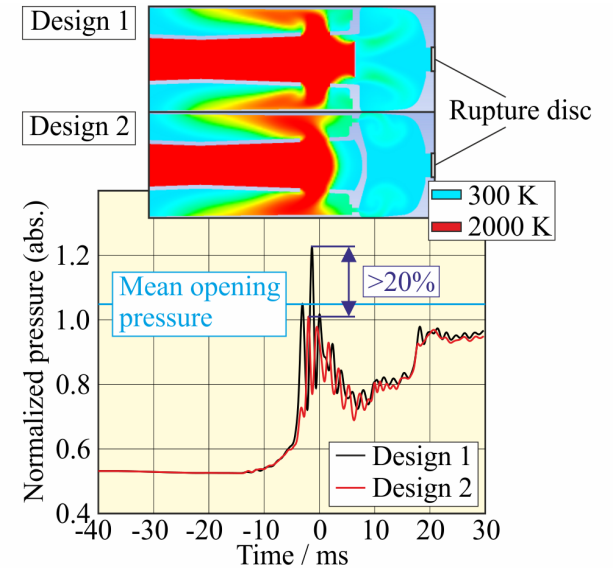

Figure 16. Pressure build-up at the rupture disc and contour plot of temperature at current zero ($t = 0$).

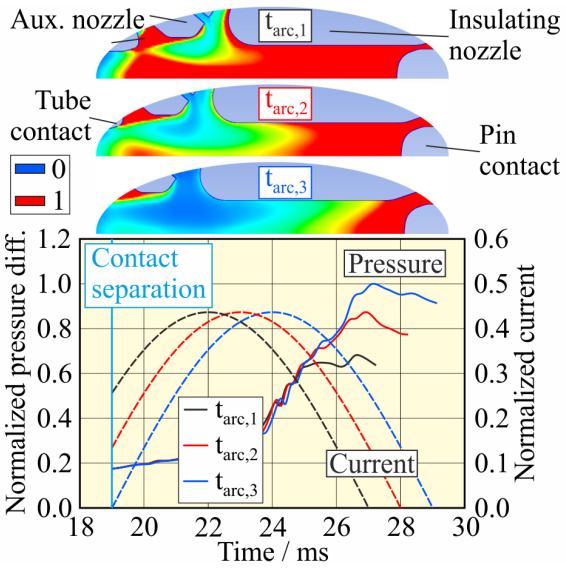

Figure 17. Distribution of dielectric criterion in the arcing volume at maximum value of TRV and corresponding trends of current and pressure in the heating volume.

of the simulated pressure at the rupture disc clearly exceeds the opening pressure identifying the necessity for a design improvement. By the modification of the interrupter unit geometry in a second design (design 2) the maximum value of the simulated pressure at the rupture disc could be reduced by about 20% (see the red curve in Figure 16). The comparison of the contour plots of temperature in Figure 16 shows that in case of design 2 the hot gas cannot flow directly into the cover. Thus the inflow of hot gas into the cover is reduced and with it the pressure rise at the rupture disc.

3.3. Estimation of minimal arcing time at TF interruption

With the approach for the study of the dielectric breakdown probability presented in Section 2.2.5 a first estimation of the minimal arcing time at TF interruption in a virtual prototype of a high-voltage circuit-breaker can be performed using the CFD arc simulation tool. Figure 17 shows for three different current trends with increasing arcing time the distribution of dielectric criterion in the arcing volume at the time when the TRV reaches its maximum value. The completely red region of the dielectric criterion ($k \geq 1$) between pin tip and tube contact in case of the smallest arcing time $t_{\mathrm{arc},1}$ characterises a high dielectric breakdown probability. The comparison of the dielectric criterion distributions illustrates that the region with low values for the dielectric criterion increases with rising arcing time. At the arcing time $t_{\mathrm{arc},3}$ almost the complete arcing volume shows low values for the dielectric criterion characterising a low dielectric breakdown probability. These simulation results lead to a minimal arcing time for the investigated virtual prototype between $t_{\mathrm{arc},2}$ and $t_{\mathrm{arc},3}$.

As it can be seen from Figure 17 the pressure build-up in the heating volume increases also with rising arcing time. The high pressure build-up in the heating volume at $t_{\mathrm{arc},3}$ forces a very strong gas flow back from the heating volume towards arcing volume at current zero. Thus, the region between the pin and the tube contact is almost completely filled with cold gas leading to high values of the critical electric field E_{cr} and to low values of the dielectric criterion k.

4. Conclusions and outlook

The present paper focuses on the basics of CFD arc simulation tools and its application with respect to the simulation of the fluid mechanical processes in the interrupter unit of SF_6 high-voltage circuit-breakers. Following the analysis of the switching-off process in a SF_6 self-blast circuit-breaker the physical system is structured which is based on the combination and interaction of several sub systems. Next, the modelling in the separated sub systems and aspects to the implementation of CFD arc simulation tools are discussed in detail. The set-up of a CFD arc simulation tool based on the program package ANSYS/FLUENT is introduced. The presented set-up does not consider electrode evaporation. It is demonstrated how this CFD arc simulation tool can be used to describe the switching-off process in a model chamber, the influence of the nozzle degradation on the pressure build-up inside the interrupter unit and the SLF interruption capacity of a real SF_6 self-blast circuit-breaker. Finally, case examples for the application of the presented CFD arc simulation tool in the development process of high-voltage circuit-breakers are illustrated.

Starting from the presented level of modelling

the capability of CFD arc simulation tools could be further improved with respect to the high-current phase e.g. by introducing a model for the electrode erosion. Essentially, this would involve the consideration of solid electrodes, the description of arc roots and metal vapour generation and the enhancement of the real gas mixture model by the new metal species. A further important improvement could be the consideration of the deviation from LTE especially in the modelling for the post arc phase. However, it can be expected that these improvements will increase both the complexity of the CFD arc simulation tool and the numerical effort resulting in longer computation times.

References

[1] M. Kriegel et al. Simulation and calculation as verification tools. *Electra*, 234:13–18, 2007.

[2] J. Sedlacek et al. Optimization of high-voltage self-blast interrupters by gas flow and electric field computations. *IEEE Transactions on Power Delivery*, 18(4):1228–1234, 2003. doi:10.1109/TPWRD.2003.817536.

[3] N. Osawa et al. Investigation of the optimum design of thermal puffer type gas circuit breaker with secondary chamber. In *15th International Conference on Gas Discharges and their Applications*, pages 13–16, Toulouse, France, 2004.

[4] F. Reichert et al. Modellierung und Simulation eines Federspeicher-Antriebssystems. *Konstruktion*, 64(3):67–73, 2012.

[5] F. Reichert. *Numerische Simulation strömungsmechanischer Vorgänge in SF_6-Hochspannungsleistungsschaltern*. Postdoctoral thesis. University press Ilmenau, Germany, 2014.

[6] J. Ostrowski et al. Computational magnetohydrodynamics in the simulation of gas circuit breakers. *International Journal of Computational Science and Engineering*, 9(5/6):433–444, 2014. doi:10.1504/IJCSE.2014.064528.

[7] C. Lüders. *Vergleich von Strahlungs- und Turbulenzmodellen zur Modellierung von Lichtbögen in SF_6-Selbstblasleistungsschaltern*. Thesis. RWTH Aachen, Germany, 2005.

[8] L. Niemeyer. Evaporation dominated high current arcs in narrow channels. *IEEE Transactions on Power Apparatus and Systems*, PAS-97(3):950–958, 1978. doi:10.1109/TPAS.1978.354568.

[9] P. Kovitya et al. Theoretical predictions of ablation-stabilised arcs confined in cylindrical tubes. *J. Phys. D: Appl. Phys.*, 17(6):1197–1212, 1984. doi:10.1088/0022-3727/17/6/016.

[10] M. Seeger et al. An integral arc model for ablation controlled arcs based on CFD simulations. *J. Phys. D: Appl. Phys.*, 39(10):2180–2191, 2006. doi:10.1088/0022-3727/39/10/029.

[11] M. Claessens et al. Simulation of gas flow phenomena in high-voltage self-blast circuit breakers at heavy fault current interruption. *IEEE Transactions on Plasma Science*, 25(5):1001–1007, 1997. doi:10.1109/27.649618.

[12] J.J. Gonzalez et al. PTFE vapor contribution to pressure changes in high-voltage circuit breakers. *IEEE Transactions on Plasma Science*, 43(8):2703–2714, 2015. doi:10.1109/TPS.2015.2450536.

[13] A. Petchanka et al. Modelling of the deformation of PTFE-nozzles in a high voltage circuit breaker due to multiple interruptions. *J. Phys. D: Appl. Phys.*, 49(13):135201, 2016. doi:10.1088/0022-3727/49/13/135201.

[14] Y.J. Kim et al. SF_6 arc plasma simulation and breakdown performance prediction using computational fluid dynamics and arc modelingoriginal. *Thin Solid Films*, 521:206–211, 2012. doi:10.1016/j.tsf.2011.11.076.

[15] M.J. Ha et al. Simulation of hot gas flow in a high voltage circuit breaker with P1 radiation model. In *20th Symposium on Physics of Switching Arc*, pages 167–171, Brno, Czech Republic, 2013.

[16] A.A. Iordanidis et al. Self-consistent radiation-based simulation of electric arcs: II. Application to gas circuit breakers. *J. Phys. D: Appl. Phys.*, 41(13):135206, 2008. doi:10.1088/0022-3727/41/13/135206.

[17] F. Reichert et al. Modelling and simulation of radiative energy transfer in high-voltage circuit breakers. *J. Phys. D: Appl. Phys.*, 45(37):375201, 2012. doi:10.1088/0022-3727/45/37/375201.

[18] P. Freton et al. Magnetic field approaches in dc thermal plasma modelling. *J. Phys. D: Appl. Phys.*, 44(34):345202, 2011. doi:10.1088/0022-3727/44/34/345202.

[19] J.J. Lowke et al. A simplified unified theory of arcs and their electrodes. *J. Phys. D: Appl. Phys.*, 30(14):2033–2042, 1997. doi:10.1088/0022-3727/30/14/011.

[20] L.Z. Schlitz et al. High-resolution transmission electron microscopy of some $Ti_{n+1}AX_n$ compounds (n=1, 2; A=Al or Si; X=C or N). *J. Appl. Phys.*, 85(5):2540–2546, 1999. doi:10.1063/1.371089.

[21] A.B. Murphy. A self-consistent three-dimensional model of the arc, electrode and weld pool in gas-metal arc welding. *J. Phys. D: Appl. Phys.*, 44(19):194009, 2011. doi:10.1088/0022-3727/44/19/194009.

[22] J.D. Yan et al. A comparative study of turbulence models for SF_6 arcs in a supersonic nozzle. *J. Phys. D: Appl. Phys.*, 32(12):1401–1406, 1999. doi:10.1088/0022-3727/32/12/317.

[23] R. Bini et al. Arc-induced turbulent mixing in an SF_6 circuit breaker model. *J. Phys. D: Appl. Phys.*, 44(2):25203–25212, 2011. doi:10.1088/0022-3727/44/2/025203.

[24] J.J. Gonzalez et al. Turbulence and magnetic field calculations in high-voltage circuit breakers. *IEEE Transactions on Plasma Science*, 40(3):936–945, 2012. doi:10.1109/TPS.2011.2180404.

[25] X. Li et al. Breakdown electric field calculation of hot SF_6 and its application to high voltage circuit breakers. In *58th IEEE Holm Conference on Electrical Contacts*, pages 43–48, Portland, OR, US, 2012.

[26] M. Yousfi et al. Breakdown electric fields in dissociated hot gas mixtures of sulfur hexafluoride including teflon: Calculations with experimental validations and utilization in fluid dynamics arc simulations. *J. Appl. Phys.*, 121(10):103302, 2017. doi:10.1063/1.4977864.

[27] S. Aded Hussein et al. Detailed investigation of breakdown prediction models for high voltage circuit breakers. *Plasma Physics and Technology*, 2(2):108–111, 2015.

[28] J.C. Lee et al. Numerical study on switching arcs and turbulence models inside a SF_6 self-blast interrupter. In *20th Symposium on Physics of Switching Arc*, pages 232–235, Brno, Czech Republic, 2013.

[29] H.K. Kim et al. Analysis of SLF interruption performance of self-blast circuit breaker by means of CFD calculation. *J. Electr. Eng. Technol.*, 9(1):254–258, 2014. doi:10.5370/JEET.2014.9.1.254.

[30] F. Reichert et al. Studies on the thermal re-ignition in SF_6 high-voltage circuit-breakers by means of coupled simulation. *Plasma Physics and Technology*, 2(2):195–198, 2015.

[31] C. Rümpler et al. Arc modeling challenges. *Plasma Physics and Technology*, 2(3):261–270, 2015.

[32] S. Hartridge et al. Aspects of plasma simulations in STAR-CCM+. NAFEMS World Congress, Stockholm, Sweden, 2016.

[33] R. Methling et al. Spectroscopic study of arc temperature profiles of a switching-off process in a model chamber. *Plasma Physics and Technology*, 2(2):163–166, 2015.

[34] A. Petchanka et al. CFD arc simulation of a switching-off process in a model chamber. *Plasma Physics and Technology*, 2(1):63–66, 2015.